Effect of oxide and nitride films on strength of silicon: A study using controlled small-scale flaws

Yeon-Gil Jung, Antonia Pajares, and Brian R. Lawn[a)]
Materials Science and Engineering Laboratory, National Institute of Standards and Technology, Gaithersburg, Maryland 20899-8500

(Received 17 June 2004; accepted 3 September 2004)

Strength properties of silicon substrates containing dense oxide and nitride surface films are investigated using nanoindentations to introduce small flaws of predetermined scale. The indentation flaws provide favored sites for failure in subsequent flexure loading, even in the subthreshold region for indentations without visible corner cracking, confirming that microflaws generated within the indentation zone act as effective crack sources in the substrate. Deposition of the oxide films increases the strength while the nitride films diminish it at any given indentation load. The strength shifts are attributed primarily to the presence of residual compressive stress in the oxide, tensile stress in the nitride. A fracture mechanics formulation based on a previous analysis for monolithic substrates is here adapted to allow for a superposed crack closing or opening stress-intensity factor term associated with the residual stresses. Allowance is also made in the mechanics for the influence of the film on effective hardness and modulus of the substrate. The formulation accounts for the basic strength shifts and enables evaluation of the magnitude of the residual stresses. The results quantify the susceptibility of basic device materials to damage from small-scale contacts and impacts.

I. INTRODUCTION

The presence of thin films is of practical importance in semiconductor and microelectromechanical system (MEMS) technology. Such films can profoundly influence the properties of a device material. For thin film systems in general, the mechanical properties that have been most widely studied are elastic modulus E and hardness H using nanoindentation probe techniques.[1–9] A recent study of silicon deposited with oxide and nitride films reveals distinctive trends in these two properties:[10] nitride films tend to harden and stiffen the silicon substrate; oxide films tend the opposite way.

One mechanical property that has received much less attention is strength, especially in the context of susceptibility to damage from small-scale contacts. Strength properties of pristine silicon without any films (other than $\approx$1 nm native oxide) have been recently measured.[11,12] However, the effect of thin films on strength properties is yet to be studied. It is well documented that residual stresses in the film layers can seriously deform substrates in small-scale devices,[13] but how do these residual film stresses influence the critical stresses to cause failure? There is a need to understand the basic strength-determining factors that can limit the prospective lifetime of device materials.

In this paper, we examine the role of surface films on the susceptibility of silicon to extraneous damage. Silicon is an ideal substrate material, not only because it is the industry standard for microelectronic and MEMS systems, but also because its basic strength properties are well understood. Dense thermally grown oxides and low-pressure chemical-vapor deposited (LPCVD) nitride films of prescribed thicknesses are adopted as coating systems. Nanoindentations are used to place controlled flaws of prescribed size into the film surfaces. The flexural strengths of the indented specimens are then recorded as the critical stresses to initiate failure from the indentation sites. We demonstrate that the oxide film strengthens the surface, while the nitride film weakens it. Finally, a simple fracture mechanics analysis, extended from a previous study but here incorporating the effect of the surface films, is developed to enable the residual stress state to be quantified.

II. EXPERIMENTAL

Monocrystalline silicon with highly polished (100) surfaces (<1 nm surface finish) was used as a substrate material (University Wafer, South Boston, MA). Plates

[a)]Address all correspondence to this author.
e-mail: brian.lawn@nist.gov
DOI: 10.1557/JMR.2004.0454

25 × 25 × 1 mm were cut from the as-supplied wafers. Surfaces were coated with two kinds of dense thin films: (i) oxide, by thermal oxidation (moist oxygen at 1100 °C); and (ii) nitride, by low-pressure chemical vapor deposition (LPCVD, SiH_2Cl_2/NH_3 gas at 830 °C). Films ranging in thickness from $d = 50$ nm to 1.2 μm were deposited, somewhat larger than generally used in device technology but expedient for highlighting effects on strength. Previous characterization by x-ray diffraction (XRD) and atomic force microscopy (AFM) of the oxide and nitride films indicated an amorphous state with no increase in surface roughness from the deposition and no detectable porosity.[10]

Nanoindentations (Nanoindenter XP, MTS Systems Corp., Oakridge, TN) were placed in the specimen surfaces using a Berkovich diamond (tip radius < 100 nm). These were made at a fixed strain rate 0.05 s^{-1}, such that each test lasted approximately 4 min over the loading half-cycle, with hold time 10 s at peak displacement and approximately 20 s unload time. All indents were made in air. Similar indentations were made on the "pristine" as-polished silicon surfaces as a comparative baseline. Presumably, these surfaces contain a relatively thin native oxide film ≈1 nm thick. Elastic modulus E and hardness H were routinely evaluated from the indentation load–displacement (P–h) curves,[14] for a range of peak indenter loads $P = 1$ mN to 2 N. Representative indentation sites were examined using AFM (Digital Instruments Nanoscope IIIa, Veeco Metrology, Santa Barbara, CA) with a gold-coated silicon nitride tip in contact mode.

Strengths of the plates were measured in a bilayer test configuration (Fig. 1).[15,16] The indented surfaces were inverted and glued face down to transparent polycarbonate support bases 12.5 mm thick with a thin (10 μm) layer of epoxy resin. Some plates were bonded without preindentation to determine strengths of surfaces with natural (polishing) flaws. The plates were mounted onto a specimen stage of a mechanical testing machine (Instron 8500, Instron Corp., Boston, MA) and loaded at the top surface with a tungsten carbide sphere of radius 3.18 mm, taking special care to align the indentation sites along the load axis. The plates were viewed with an inverted video camera arrangement from below the polycarbonate base[15] to ascertain the source of fracture, i.e., indentation site or natural flaw. Strengths were calculated from $S = (L/BD^2)\log(E/E_P)$, where L is the load at failure, D is plate thickness, E is modulus of the upper plate and $E_P = 3.25$ GPa modulus of the polycarbonate, and $B = 1.35$.[17] This relation neglects the presence of the thin film and assumes that failure initiates in the substrate. In this way, strength S was measured as a function of indentation load P for specimens with different films and thicknesses d. The bilayer strength test configuration in Fig. 1 samples only a small volume immediately around the indentation site, conveniently avoiding edge and support failures. However, as with most strength tests, it allows only one test result per specimen.

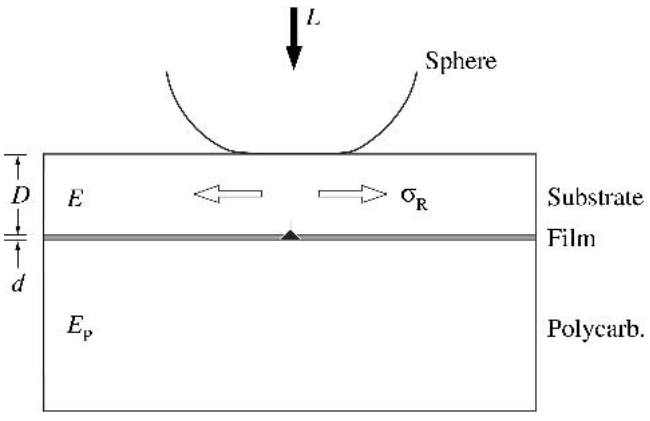

FIG. 1. Bilayer test configuration, showing ceramic plate of thickness D with film of thickness d bonded to polycarbonate support. Plate contains a Berkovich diamond nanoindentation at its lower surface, with a residual stress σ_R, and is loaded at its top surface with concentrated force L. Tensile stresses at plate undersurface are localized around centrally aligned indentation site.

III. THEORETICAL MODEL FOR STRENGTH DEGRADATION

A. Background

A simplified fracture mechanics analysis for initiation of failure from incipient microcracks within quasiplastic indentation damage zones has previously been developed for monolithic materials and validated using strength data on silicon substrates containing nanoindentations.[12] In this section we adapt that analysis to allow for the presence of a film of thickness d at the indentation surface. The film is presumed to contain a residual stress σ_R from film/substrate thermal expansion mismatch. For relatively thin films, any counterbalancing stresses in the substrate may be considered negligible. Such film residual stresses may be expected to enhance or inhibit any ensuing cracking in the substrate, depending on whether these stresses are tensile or compressive.

The film/substrate is subjected to contact with a sharp indenter at load P, contact dimension a (distance from center to corner), penetration h (Fig. 2). The hardness of the substrate is[14,18]

$$H = P/\alpha a^2 = P/\alpha' h^2 \quad , \tag{1}$$

with α and α' dimensionless coefficients. In the approximation $a \gg d$, the bulk of the elastic-plastic deformation resides in the substrate. The principal role of the film is then to exert an opening or closing force on any cracks initiating in the substrate. However, this approximation is less valid in the sub-threshold flaw region, and we shall later incorporate a correction term to allow for the

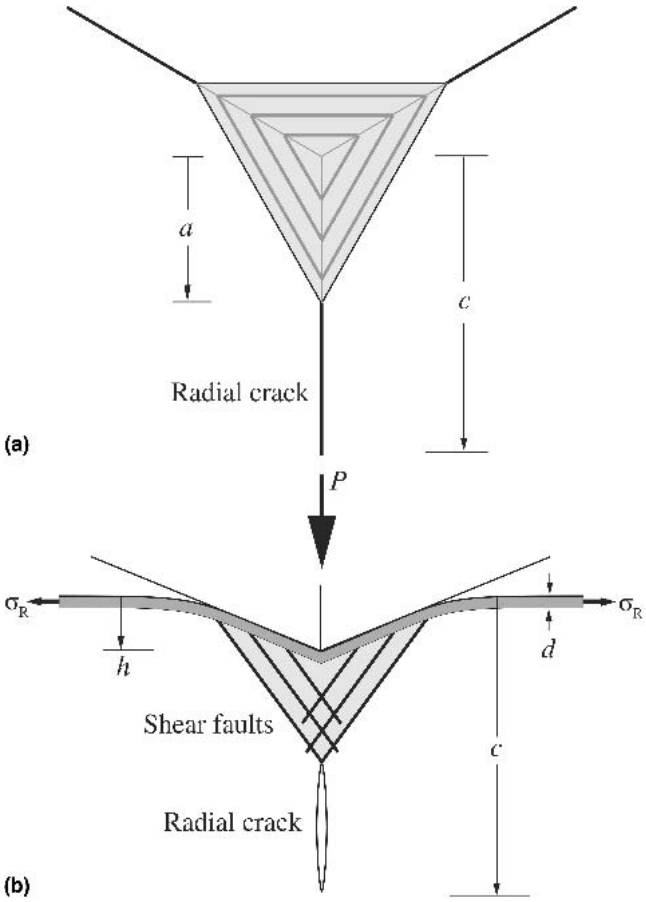

FIG. 2. Schematic showing sharp indentation at load P, contact dimension a, penetration h, onto silicon plate with surface film of thickness d; (a) top view, (b) section view. Film contains residual in-plane stress σ_R. Shear faults form within deformation zone of dimension a and initiate radial cracks of dimension c.

modifying effect of the film on effective hardness H in this region (Sec. III. D).

The indentation develops a quasiplastic damage zone consisting of shear-induced slip faults which act as incipient sources for initiation of radial cracks in the substrate.[19–24] The essence of the simplified approach is to treat the subcritical shear faults as "equivalent" mode I cracks of size $c \approx a$.[19,20,24] At a critical load, the cracks extend initially on median places (planes normal to the surface and containing the indentation axis) below the surface and complete themselves in half-penny configurations of radius c, with radial traces on the top surface.[25] To first approximation, any distorting effects of the residual stresses on the penny-like crack geometry near the specimen surface are neglected. The goal is then to determine the strength S of the specimen containing such indentation flaws as a function of contact load P.

B. Subthreshold flaws

At sufficiently low indentation loads the indentations contain no visible radial cracks at their corners. This is the subthreshold region. In a strength test, radial crack initiation from cracklike slip faults of dimension a within the quasiplastic zone takes the system spontaneously to failure. Following the previous formalism for monolithic solids,[12] the stress-intensity factor for the equivalent microcrack flaw may be written in the generic form

$$K = \lambda\sigma a^{1/2} + \kappa H a^{1/2} + 2\psi\sigma_R d^{1/2} \quad , \qquad (2)$$

where λ, κ, and ψ are crack-geometry coefficients. The first term on the right represents the driving force from an applied tensile stress σ, in this case by bilayer flexure; the second is from an elastic-plastic residual indentation field, proportional to hardness H; the third term allows for the superposed effect of the residual stress σ_R in the film.[26,27] In this third term, for $a \gg d$ (Fig. 2), the effect of the residual stress is considered to be equivalent to an opening or closing line force $\sigma_R d$ acting on the crack trace.[26] Actually, one might include a fourth term, allowing for the presence of a residual stress of opposite sign in the substrate, but such a term is small for relatively thin films and is neglected here.[27]

On increasing the applied stress σ, the flaw remains stationary until $K = T$ (single-valued toughness, K_{IC}) is reached at a critical stress $\sigma = S$, at which point it extends unstably to failure. This condition defines the strength

$$S = (1/\lambda)[T'/a^{1/2} - \kappa H]$$
$$= (1/\lambda)[(\alpha H/P)^{1/4} T' - \kappa H] \quad , \qquad (3)$$

using Eq. (1), where T' defines an "effective toughness"

$$T' = T - 2\psi\sigma_R d^{1/2} \quad . \qquad (4)$$

The definition of Eq. (4) reduces the relations in Eq. (3) to the same form as for a substrate without any film, with T' replacing T.[12] In this formulation, the effect of the residual stress σ_R is simply to diminish or enhance the effective toughness T' of the substrate material, depending on whether σ_R is tensile or compressive. Since the radial crack is presumed to initiate in the substrate, T in Eq. (4) pertains to the substrate material. However, the presence of the film will influence the "effective hardness" H in Eq. (3); allowance for this influence will be made in Sec. III. D.

The limiting condition $S = 0$ in Eq. (3) defines the threshold contact size $a = a_*$ for spontaneous radial cracking, i.e. in the absence of any applied stress:

$$a_* = (T'/\kappa H)^2 \qquad (5a)$$

$$P_* = 2T'^4/\kappa^4 H^3 \quad . \qquad (5b)$$

C. Postthreshold flaws

Beyond the threshold at $a > a_*$, fracture initiates spontaneously from the indentation corners prior to application of any applied tensile loading, and arrests in the

well-known radial crack formation with characteristic size c. The stress-intensity factor for the well-developed radial crack in subsequent biaxial loading has the same form as Eq. (2) above, but with the second term on the right replaced by $\chi P/c^{3/2}$, where χ is an elastic-plastic stress-field coefficient[25,28–30]

$$K = \psi\sigma c^{1/2} + \chi P/c^{3/2} + 2\psi\sigma_R d^{1/2} \quad . \tag{6}$$

On increasing the applied stress, the radial crack propagates stably to a critical size at $dK/dc = 0$, $K = T$, defining the strength $\sigma = S$[12,25,28]

$$S = \beta(T'^4/P)^{1/3} \quad , \tag{7}$$

where $\beta = (3/4\psi)(1/4\chi)^{1/3}$. Again, the equations have the same form as for monolithic substrates, but with T' replacing T.

D. Effects of hardness and modulus variations

Allusion was made above to a dependence of hardness H on load P for substrates with a film of thickness d. As indentation penetration h diminishes, the indentation field samples a greater proportion of the film, so that H deviates increasingly from that of the substrate. For a

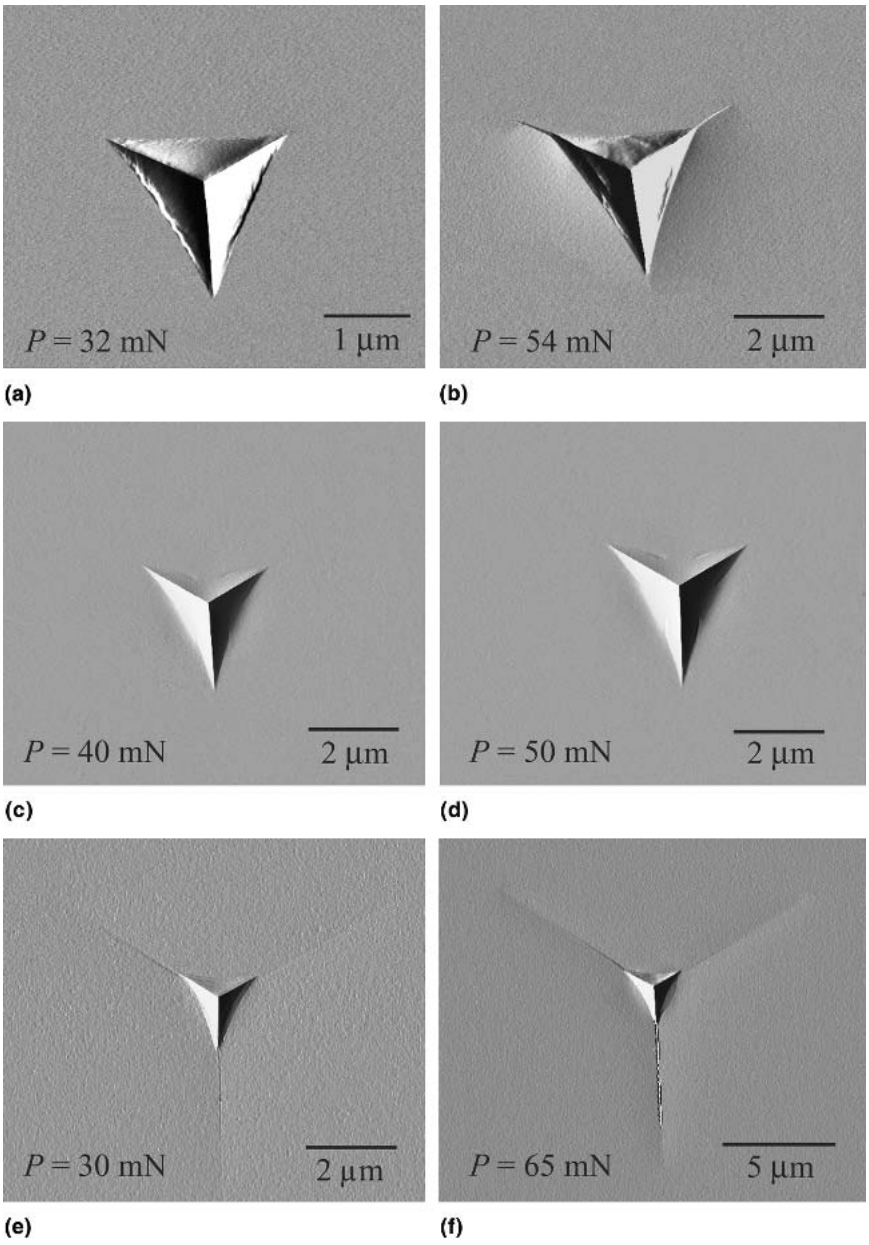

FIG. 3. AFM images of Berkovich nanoindentations in silicon (100), at loads shown: (a,b) with pristine (as-polished) surface; (c,d) with oxide surface film, thickness $d = 580$ nm; and (e,f) with nitride surface film, $d = 780$ nm. Note relative suppression of cracking in oxide films, enhancement in nitride films.

given indentation load P, such deviations will influence H, the more so for smaller h and larger d. It follows that any such modifications are most likely to be felt in the subthreshold flaw region. Allowance for this factor may be made using an existing empirical relation for effective hardness H in terms of relative indenter penetration h/d[10]

$$H = H_s(H_f/H_s)^M \quad , \tag{8}$$

where H_s and H_f refer to the substrate and film, respectively, and the exponent term M is a geometrical function

$$M = 1/[1 + B'(h/d)^{D'}] \quad . \tag{9}$$

The values $B' = 1.47$ and $D' = 1.71$ are found to give a reasonable fit to hardness data for the film systems of interest here, with $H_s = 12.7$ GPa (silicon), $H_f = 11.5$ GPa (oxide), and $H_f = 35.0$ GPa (nitride).[10]

Equation (9) can also be expressed in terms of indentation load P, using Eq. (1) to eliminate h. Combination of Eqs. (1), (8), and (9) with Eqs. (2), (3), and (5) then corrects for the influence of film properties on the subthreshold strength relations.

The post-threshold region of well-developed radial cracks is much less sensitive to film influence. The elastic-plastic coefficient in eqn. 6 has the form $\chi \propto (E/H)^{1/2}$, with E Young's modulus.[29] Like H, E is dependent on film thickness h, in a manner analogous to Eqs. (8) and (9).[10] However, the coefficient β that determines strength in Eq. (7) depends only on $\chi^{-1/3}$ or $(E/H)^{-1/6}$, in which case any such variations may be considered insignificantly small.

IV. RESULTS AND ANALYSIS

Figure 3 shows AFM images of Berkovich indentations for monolithic (100) silicon and silicon with oxide and nitride films in two load ranges, $P = 30$ to 40 mN (left) and $P = 50$ to 65 mN (right) (equivalent to contact penetration ranges $h = 300$ to 500 nm and $h = 500$ to 600 nm). In monolithic silicon [Figs. 3(a) and 3(b)], the indentations shown span the threshold for visible radial cracking at impression corners: i.e., no visible cracking in Fig. 3(a), corner cracking in Fig. 3(b). In silicon with oxide film [Figs. 3(c) and 3(d)], neither of the indentation images show corner cracking. In silicon with nitride film [Figs. 3(e) and 3(f)], on the other hand, corner cracks are apparent in both images and are relatively large. Thus the oxide suppresses the threshold for cracking while the nitride enhances it.

Figures 4 and 5 are plots of strength S versus maximum Berkovich indenter load P for silicon with dense oxide and nitride films, respectively. Each figure contains data for specified film thicknesses d. Individual data points represent single tests.[12] Both figures include data for monolithic silicon as a reference baseline. Filled symbols represent breaks from indentation flaws, unfilled symbols breaks from natural flaws. Shaded boxes at the left axis show mean and standard deviation strengths for >25 specimens, monolithic and deposited, on control specimens without indentations. Data for breaks from

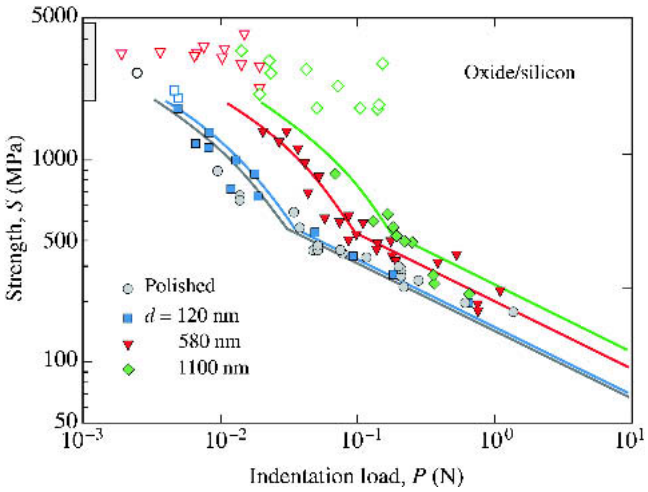

FIG. 4. Strength S of silicon plates containing oxide films of specified thicknesses d, as function of indentation load P. Data points represent breaks from indentations (filled symbols), or from natural flaws (unfilled symbols). Solid curves are data fits to Eq. (3) (subthreshold) and Eq. (7) (postthreshold). Shaded box at left axis is mean and standard deviation for specimens without indentations.

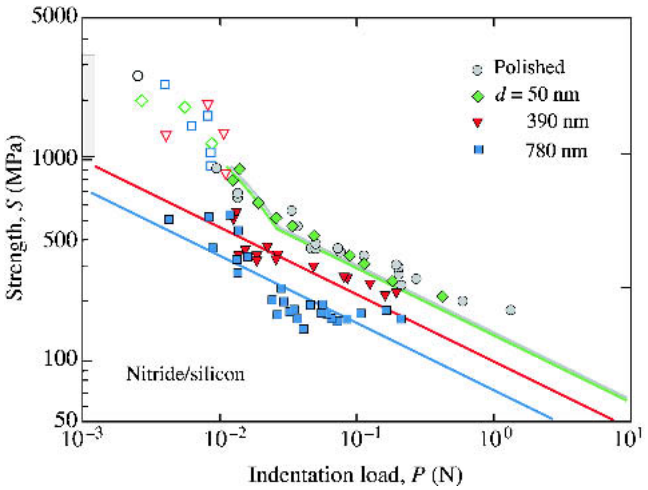

FIG. 5. Strength S of silicon plates containing nitride films of specified thickness d, as function of indentation load P. Data points represent breaks from indentations (filled symbols), or from natural flaws (unfilled symbols). Solid lines are data fits to Eq. (3) (subthreshold) and Eq. (7) (postthreshold). Shaded box at left axis is mean and standard deviation for specimens without indentations.

postthreshold indentations with excessive chipping[12] are omitted from the plots. The data shifts clearly indicate strengthening and weakening effects for the oxide and nitride films, respectively. Note the large scatter for data from thicker films, suggesting perhaps some loss in film integrity in this thickness region.

Solid lines through the data in Figs. 4 and 5 are curve fits using Eqs. (3) and (7), in conjunction with Eqs. (1), (8), and (9). First, regression fits are made to the monolithic silicon data for indentation-site failures, using $T' = T = 1.1$ MPa$^{1/2}$ for silicon and adjusting the coefficients $\lambda = 0.45$ and $\kappa = 0.058$ in the subthreshold region and $\beta = 1.25$ in the postthreshold region. [These parameter evaluations are only slightly different to those in a previous study of (111) surfaces,[12] corresponding to a small upward data shift along the S axis.] Fits to the data sets for silicon with films are then made using the same coefficients but adjusting T' for each value of d. In this latter case, we insert $\alpha = 1.30$ and $\alpha' = 13.0$ for Berkovich indenters into Eq. (1), corresponding to contact dimension a measured from indentation corner to center and peak-load penetration h measured from indentation surface[18] (neglecting any pile-up around the indenter—good for hard, brittle materials[31]). Note that in Fig. 5, the threshold for the substrates with thicker films is displaced to the left of the data range.

Values of T' with standard deviation error bars are plotted as a function of root film thickness $d^{1/2}$ in Fig. 6, in accordance with Eq. (4). Linear fits to the data [assuming $\psi = 1$ in Eq. (4)][26] then yield estimates of the residual stresses in each film type, i.e., $\sigma_R = -233 \pm 58$ MPa for the oxide and $\sigma_R = +228 \pm 68$ MPa for the nitride (mean and standard deviation).

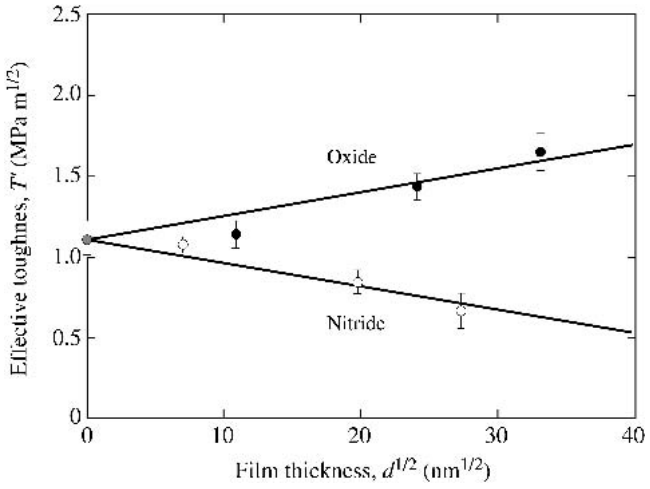

FIG. 6. "Effective toughness" T' as function of root film thickness $d^{1/2}$, for silicon substrates with oxide and nitride films. Solid lines are fits to Eq. (4).

V. DISCUSSION AND CONCLUSIONS

We have measured strengths S of silicon with dense oxide and nitride surface films of specified thicknesses d containing nanoindentations made at load P. Whereas the oxide film enhances strength (Fig. 4), the nitride film degrades it (Fig. 5). The strength shifts correspond to an increase (oxide) or decrease (nitride) in the threshold loads for radial cracking, as indicated by the intersection of the subthreshold and postthreshold curves and as observed in the images of Fig. 3. A fracture mechanics model has been developed to account for the strength shifts, based on the notion that residual stresses within the film act to close or open cracks in the silicon substrate. The influence of the residual stresses σ_R is subsumed into an effective substrate toughness term T' in Eq. (4), which replaces the intrinsic toughness T for monolithic materials in Eqs. (3), (5), and (7).

The data shifts in the strength plots in Figs. 4 and 5 have been used to evaluate the residual stresses for each film type. Evaluations made this way may be compared with those calculated from a relation for stresses in bilayers with thermal expansion mismatch, $\sigma_R = (\alpha_f - \alpha_s)E_f\Delta T/(1 - \nu_f)$,[32,33] inserting the following parameters: film expansion coefficients $\alpha_f = 0.5 \times 10^{-6}$ °C^{-1} (fused silica) and $\alpha_f = 3.6 \times 10^{-6}$ °C^{-1} (silicon nitride),[34] substrate coefficient $\alpha_s = 2.5 \times 10^{-6}$ °C^{-1} (silicon);[35] film moduli $E_f = 70$ GPa (fused silica) and $E_f = 170$ GPa for (silicon nitride), along with common Poisson's ratios $\nu_f = 0.22$. This relation yields $\sigma_R = -189$ MPa (oxide) and $\sigma_R = +314$ MPa (nitride), which compare with $\sigma_R = -233 \pm 58$ MPa (oxide) and $\sigma_R = +228 \pm 68$ MPa (nitride) from the data fits in Fig. 6. Given the scatter of data in Figs. 4 and 5, along with limitations in the fracture mechanics formulation (see below), the quantitative determinations from the current strength data should probably be regarded as no more than estimates.

Once the parameters λ, κ, and β in Eqs. (3) and (7) have been "calibrated" for a given substrate material, the same equations can be used to predict the strength response $S(P)$ for any film of given thickness d and mismatch residual stress σ_R. However, in using the fracture mechanics analysis, it is well to be aware of several limitations in the underlying assumptions. It can be envisioned that film toughness properties can become important, even dominant, at ultra-small contacts. Then, in considering the opening or closing influence of the film residual stress in the fracture mechanics, it is assumed that the cracks retain an essential penny-like character. Instead, the cracks must splay out or pinch in near the top surface so that, strictly, the analysis should include an additional geometrical modification factor. As a result of these assumptions, our method is probably not a reliable means of quantifying film residual stresses, but

nevertheless remains a valuable indicator of trends in strength properties for film systems fabricated under different deposition conditions.

ACKNOWLEDGMENTS

This work was sponsored by NIST internal funds, by a grant to Yeon-Gil Jung from the Korea Institute S & T Evaluation and Planning (KISTEP) through the National Research Laboratory, and by a grant to Antonia Pajares from the Ministerio de Ciencia y Tecnologia of Spain (MAT2003-05584).

Information of product names and suppliers in this paper is not to imply endorsement by NIST.

REFERENCES

1. P.M. Sargent: In *Micro Indentation Hardness Testing*, edited by P.J. Blau and B.R. Lawn (ASTM Special Technical Publication **899,** ASTM, Philadelphia, PA, 1986), pp. 160–174.
2. P.J. Burnett and D.S. Rickerby: The mechanical properties of wear-resistant coatings. I. Modeling of hardness behavior. *Thin Solid Films* **148,** 41 (1987).
3. P.J. Burnett and D.S. Rickerby: The mechanical properties of wear-resistant coatings. II. Experimental studies and interpretation of hardness. *Thin Solid Films* **148,** 51 (1987).
4. A.K. Bhattacharya and W.D. Nix: Analysis of elastic and plastic deformation associated with indentation testing of thin films on substrates. *Int. J. Solids Struct.* **24,** 1287 (1988).
5. H. Gao, C-H. Chiu, and J. Lee: Elastic contact versus indentation modelling of multi-layered materials. *Int. J. Solids Struct.* **29,** 2471 (1992).
6. P-L. Larsson and I.R.M. Peterson: Evaluation of sharp indentation testing of thin films and ribbons on hard substrates. *J. Test. Eval.* **30,** 64 (2002).
7. T.Y. Tsui, C.A. Ross, and G.M. Pharr: A method for making substrate-independent hardness measurements of soft metallic films on hard substrates by nanoindentation. *J. Mater. Res.* **18,** 1383 (2003).
8. B. Bhushan: Nanomechanical characterization of solid surfaces and thin films. *Int. Mater. Rev.* **48,** 125 (2003).
9. A. Perriot and E. Barthel: Elastic contact to a coated half-space: Effective elastic modulus and real penetration. *J. Mater. Res.* **19,** 600 (2004).
10. Y-G. Jung, B.R. Lawn, M. Martyniuk, H. Huang, and X. Hu: Evaluation of elastic modulus and hardness of thin films by nanoindentation. *J. Mater. Res.* **19,** 3076 (2004).
11. A. Pajares, M. Chumakov, and B.R. Lawn: Strength of silicon containing nanoscale flaws. *J. Mater. Res.* **19,** 657 (2004).
12. Y-G. Jung, A. Pajares, R. Banerjee, and B.R. Lawn: Strength of silicon, sapphire and glass in the subthreshold flaw region. *Acta Mater.* **52,** 3459 (2004).
13. L.B. Freund and S. Suresh: *Thin Film Materials: Stress, Defect Formation and Surface Evolution* (Cambridge University Press, Cambridge, U.K., 2004).
14. W.C. Oliver and G.M. Pharr: An improved technique for determining hardness and elastic-modulus using load and displacement sensing indentation experiments. *J. Mater. Res.* **7,** 1564 (1992).
15. H. Chai, B.R. Lawn, and S. Wuttiphan: Fracture modes in brittle coatings with large interlayer modulus mismatch. *J. Mater. Res.* **14,** 3805 (1999).
16. Y-W. Rhee, H-W. Kim, Y. Deng, and B.R. Lawn: Contact-induced damage in ceramic coatings on compliant substrates: Fracture mechanics and design. *J. Am. Ceram. Soc.* **84,** 1066 (2001).
17. P. Miranda, A. Pajares, F. Guiberteau, Y. Deng, and B.R. Lawn: Designing damage-resistant brittle-coating structures: I. Bilayers. *Acta Mater.* **51,** 4347 (2003).
18. A.C. Fischer-Cripps: *Nanoindentation* (Springer-Verlag, New York, NY 2002).
19. B.R. Lawn, T.P. Dabbs, and C.J. Fairbanks: Kinetics of shear-activated indentation crack initiation in soda-lime glass. *J. Mater. Sci.* **18,** 2785 (1983).
20. H.M. Chan and B.R. Lawn: Indentation deformation and fracture of sapphire. *J. Am. Ceram. Soc.* **71,** 29 (1988).
21. J.G. Bradby, J.S. Williams, J. Wong-Leung, M.V. Swain, and P. Munroe: Mechanical deformation in silicon by micro-indentation. *J. Mater. Res.* **16,** 1500 (2001).
22. J.G. Bradby, J.S. Williams, J. Wong-Leung, S.O. Kucheyev, M.V. Swain, and P. Munroe: Spherical indentation of compound semiconductors. *Philos. Mag. A* **82,** 1931 (2002).
23. I. Zarudi, L.C. Zhang, and M.V. Swain: Microstructure evolution in monocrystalline silicon in cyclic microindentations. *J. Mater. Res.* **18,** 758 (2003).
24. B.R. Lawn: Fracture and deformation in brittle solids: A perspective on the issue of scale. *J. Mater. Res.* **19,** 22 (2004).
25. D.B. Marshall and B.R. Lawn: Residual stress effects in sharp-contact cracking: I. Indentation fracture mechanics. *J. Mater. Sci.* **14,** 2001 (1979).
26. B.R. Lawn and E.R. Fuller: Measurement of thin-layer surface stresses by indentation fracture. *J. Mater. Sci.* **19,** 4061 (1984).
27. M.F. Gruninger, B.R. Lawn, E.N. Farabaugh, and J.B. Wachtman: Measurement of residual stresses in coatings on brittle substrates by indentation fracture. *J. Am. Ceram. Soc.* **70,** 344 (1987).
28. D.B. Marshall, B.R. Lawn, and P. Chantikul: Residual stress effects in sharp-contact cracking: II. Strength degradation. *J. Mater. Sci.* **14,** 2225 (1979).
29. B.R. Lawn, A.G. Evans, and D.B. Marshall: Elastic/plastic indentation damage in ceramics: The median/radial crack system. *J. Am. Ceram. Soc.* **63,** 574 (1980).
30. B.R. Lawn: *Fracture of Brittle Solids* (Cambridge University Press, Cambridge, U.K., 1993).
31. X. Chen and J.J. Vlassak: Numerical study on the measurement of thin film mechanical properties by means of nanoindentation. *J. Mater. Res.* **16,** 2974 (2001).
32. H. Wang and X.Z. Hu: Surface properties of ceramic laminates fabricated by die pressing. *J. Am. Ceram. Soc.* **79,** 553 (1996).
33. K.S. Lee, S.K. Lee, B.R. Lawn, and D.K. Kim: Contact damage and strength degradation in brittle/quasi-plastic silicon nitride bilayers. *J. Am. Ceram. Soc.* **81,** 2394 (1998).
34. W.D. Callister: *Materials Science and Engineering: An Introduction* (John Wiley & Sons, New York, NY, 1997).
35. D.R. Lide: In *Handbook of Chemistry and Physics* (CRC Press, Boca Raton, FL, 2003), pp. 12–97.